

Anisotropic shock sensitivity for β -octahydro-1,3,5,7-tetranitro-1,3,5,7-tetrazocine energetic material under compressive-shear loading from ReaxFF-Ig reactive dynamics simulations

Tingting Zhou, Sergey V. Zybin, Yi Liu, Fenglei Huang, and William A. Goddard

Citation: *J. Appl. Phys.* 111, 124904 (2012); doi: 10.1063/1.4729114

View online: <http://dx.doi.org/10.1063/1.4729114>

View Table of Contents: <http://jap.aip.org/resource/1/JAPIAU/v111/i12>

Published by the [American Institute of Physics](#).

Related Articles

Band-filling dependence of thermoelectric properties in B20-type CoGe
[Appl. Phys. Lett.](#) 100, 093902 (2012)

Scaling of light emission from detonating bare Composition B, 2,4,6-trinitrotoluene [C₇H₅(NO₂)₃], and PE4 plastic explosive charges
[J. Appl. Phys.](#) 110, 084905 (2011)

Mechano-chemical pathways to H₂O and CO₂ splitting
[Appl. Phys. Lett.](#) 99, 154105 (2011)

In-situ measurements of the onset of bulk exothermicity in shock initiation of reactive powder mixtures
[J. Appl. Phys.](#) 109, 084905 (2011)

Dissociation of methane under high pressure
[J. Chem. Phys.](#) 133, 144508 (2010)

Additional information on *J. Appl. Phys.*

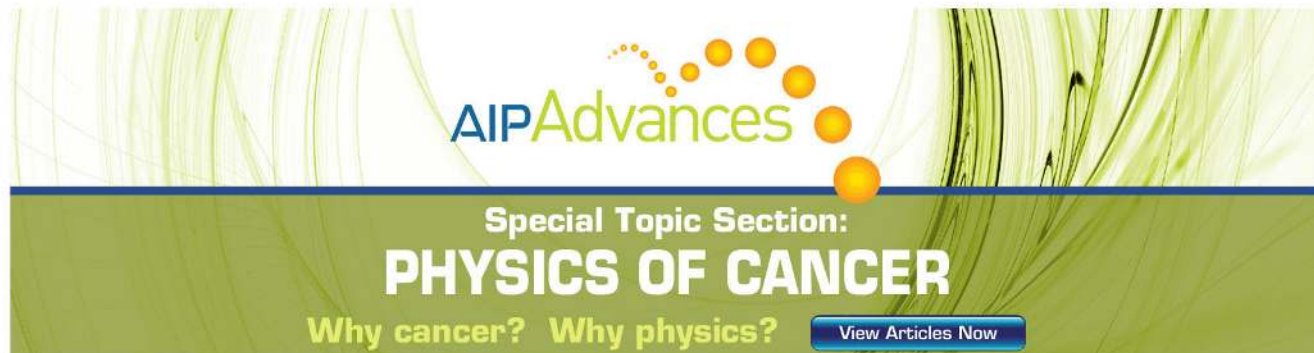
Journal Homepage: <http://jap.aip.org/>

Journal Information: http://jap.aip.org/about/about_the_journal

Top downloads: http://jap.aip.org/features/most_downloaded

Information for Authors: <http://jap.aip.org/authors>

ADVERTISEMENT



AIP Advances

Special Topic Section:
PHYSICS OF CANCER

Why cancer? Why physics? [View Articles Now](#)

Anisotropic shock sensitivity for β -octahydro-1,3,5,7-tetranitro-1,3,5,7-tetrazocine energetic material under compressive-shear loading from ReaxFF- ℓg reactive dynamics simulations

Tingting Zhou,^{1,2} Sergey V. Zybin,² Yi Liu,^{2,3} Fenglei Huang,¹ and William A. Goddard III^{2,a)}

¹State Key Laboratory of Explosion Science and Technology, Beijing Institute of Technology, Beijing 100081, People's Republic of China

²Materials and Process Simulation Center, 139-74, California Institute of Technology, Pasadena, California 91125, USA

³School of Materials Science and Engineering, University of Shanghai for Science and Technology, Shanghai 200093, People's Republic of China

(Received 1 August 2011; accepted 15 May 2012; published online 20 June 2012)

We report here the predictions on anisotropy of shock sensitivity and of chemical process initiation in single crystal β -octahydro-1,3,5,7-tetranitro-1,3,5,7-tetrazocine (β -HMX) using compressive shear reactive dynamics (CS-RD) model with ReaxFF- ℓg reactive force field. Analysis of resolved shear stress induced by uniaxial compression along three shock directions normal to (110), (011), and (010) planes leads to identify eight slip systems as candidates for shear deformation. For each of the eight slip systems, non-equilibrium reactive dynamics simulations were carried out to determine thermal, mechanical, and chemical responses to shear deformation. Shock direction normal to (010) plane exhibits large shear stress barriers arising from steric hindrance between molecules of adjacent layers leading to local dramatic energy and temperature increases under shear flow that in turn accelerate chemical bond breaking and initial product formation processes, promoting further molecular decomposition and eventually transition to detonation. This suggests that single crystal β -HMX is sensitive to shocks in direction normal to (010) plane. Shock directions normal to (110) and (011) planes reveal significantly less steric hindrance, leading to more modest energy and temperature increases followed by slower chemical reaction initiation. Thus, shock directions normal to (110) and (011) planes are less sensitive than shock direction normal to (010) plane, which agree with interpretations from currently available plate impact experiments on HMX. This validation of CS-RD and ReaxFF for characterizing sensitivity of single crystal energetic materials indicates that these methods can be applied to study sensitivity for more complex polymer bonded explosives and solid composite propellants having complex microstructures, corrugated interfaces, as well as defects. © 2012 American Institute of Physics. [<http://dx.doi.org/10.1063/1.4729114>]

I. INTRODUCTION

Energetic materials (EMs), such as octahydro-1,3,5,7-tetranitro-1,3,5,7-tetrazocine (HMX), are mixed with polymers to form polymer bonded explosives (PBX) or with oxidizer to form propellants. Important in storing and handling these materials is their sensitivity to accidental detonation. Despite numerous investigations to uncover the origins of sensitivity in these materials, there is not yet an understanding of how local structure in shock-compressed high explosives evolve to undergo very complex physical and chemical processes from shock initiation to a steady state detonation and why this can depend strongly on impurities and defects and even on shock direction.^{1,2} Interpretations from experimental studies are complicated by heterogeneities due to surfaces, voids, and inclusions, all of which may contribute to sensitivity. The characteristics of the response to shock processes strongly depend on mechanical properties (crystal orientation, microstructure, gaps, defects, interfaces,

etc.), thermodynamic properties (temperature, pressure, density, etc.), and chemical properties (molecule, composition and energetics, reaction pathways, kinetic rates, etc.) of high explosives.³ Importantly, these properties of high explosives vary rapidly with time and are often transient in nature under shock compression. Consequently, it is critical to examine the initial time-dependent data of thermal, chemical, and mechanical properties of high explosives to obtain in-depth insights into shock initiation and detonation.⁴⁻⁶

A major step forward in understanding sensitivity was the discovery by Dick⁷⁻⁹ that shocking a single crystal of pentaerythritol tetranitrate (PETN) leads to dramatic differences in sensitivity, depending on shock direction, indicating that crystal packing within a crystal must play an important role. Indeed, we recently studied shock direction dependence of PETN using compressive shear reactive dynamics (CS-RD) simulations, showing consistent results with the experimental observed dependence of sensitivity on shock direction.¹⁰ For energetic materials other than PETN, experimental evidence for shock sensitivity dependent on direction is less clear-cut, but weak shock experiments on HMX has demonstrated that shock direction normal to (010)

^{a)}Author to whom correspondence should be addressed. Electronic mail: wag@wag.caltech.edu.

plane appears to be more sensitive than shock directions normal to (110) and (011) planes.^{11,12} Thus, we decided to test on HMX the CS-RD computational model already validated for PETN.

The remainder of this paper is organized as follows: the computational protocol of CS-RD and ReaxFF reactive force field are described in Sec. II. Results and discussions are presented in Sec. III. Conclusions are drawn in Sec. IV.

II. THE CS-RD MODEL

A. Introduction

To provide an atomistic understanding of the mechanism involved in initiating detonation and affecting sensitivity, we developed a reactive dynamics (RD) simulation strategy to enable computational study of the complex processes at atomistic level.¹⁰ The computational protocol, CS-RD with ReaxFF reactive force field, was used to simulate the physical and chemical processes for PETN resulting from combined shear and compression loads.¹⁰ For crystal directions known to be sensitive, CS-RD finds large shear stress overshoots coupled with a fast increase of temperature that leads to early bond-breaking processes and fast molecular decomposition, whereas, directions known to be insensitive exhibit small shear stress overshoot, low temperature increase, and little bond dissociation. These results are consistent with those from experiments, leading to confirmation and elaboration of the steric hindrance model.¹⁰

In this paper, the CS-RD model with ReaxFF- ℓg ¹³ reactive force field was applied to study the anisotropic shock sensitivity of HMX, which is widely used in the formations of explosives and propellants.

B. The ReaxFF reactive force field

ReaxFF reactive force field has previously been applied to study the thermal and shock-induced decompositions for cyclotrimethylene trinitramine (RDX), triaminotrinitrobenzene (TATB), HMX, and PETN,^{14–19} providing valuable information on initial chemical decomposition and subsequent energy release process. ReaxFF RD simulations of reactive processes have already been reported on systems with millions of atoms,¹⁶ making it practical to study large-scale systems with currently available computational facilities.

ReaxFF- ℓg is an extension of ReaxFF, in which an additional term is added to account for London dispersion (van der Waals attraction). This provides a more accurate description of cell parameters for molecular crystals at low pressure. It has been tested for several energetic materials, including RDX, PETN, TATB, and nitromethane.¹³ The calculated crystal structures and equations of state are in good agreements with experimental results, and the description of phase diagram for RDX is improved. ReaxFF- ℓg is recently applied to calculate the crystal structures and equations of state for HMX polymorphs under hydrostatic compression, obtaining good agreements with experimental and theoretical reports.²⁰

ReaxFF- ℓg , corrects London dispersion interaction (van der Waals attraction) by adding an extra term using low-gradient model, $E_{\ell g}$, as follows:¹³

$$E_{Reax-\ell g} = E_{Reax} + E_{\ell g}$$

$$E_{Reax} = E_{bond} + E_{lp} + E_{over} + E_{under} + E_{val} + E_{pen}$$

$$+ E_{coa} + E_{tors} + E_{conj} + E_{H-bond} + E_{vdWaals} + E_{Coulomb}$$

$$E_{\ell g} = - \sum_{ij, i < j}^N \frac{C_{\ell g, ij}}{r_{ij}^6 + dR_{eij}^6}$$

Here E_{bond} corresponds to the bond dissociation energy, E_{lp} to the lone pair energy penalty based on the number of lone pairs around an atom, E_{over} to the energy penalty for over-coordinated atoms, E_{under} to the energy contribution for the resonance of the n -electron between attached undercoordinated atomic centers, E_{val} to the angle bending energy, E_{pen} to an energy penalty needed to reproduce the stability of systems with double bonds sharing an atom in a valency angle, E_{coa} to three-body conjugation term to describe the stability of $-NO_2$ groups, E_{tors} to the torsion angle energy, E_{conj} to describe the contribution of conjugation effects to the molecular energy, E_{H-bond} to the H-bond energy, $E_{vdWaals}$ to the van der Waals interaction, $E_{Coulomb}$ to the Coulomb interaction, and $E_{\ell g}$ to account for long range London Dispersion. r_{ij} is the distance between atom i and atom j , R_{eij} is the equilibrium vdW distance, and $C_{\ell g, ij}$ is dispersion energy coefficients. d is a scaling factor, which is set to be 1.0 in this work.

All calculations in this paper were performed using ReaxFF- ℓg implemented in general reactive atomistic simulation package (GRASP). To test the accuracy of ReaxFF- ℓg for β -HMX with $P2_1/n$ space group, we applied it to calculate the equilibrium crystal structure at ambient condition using isothermal-isobaric molecular dynamics (NPT-MD) simulation. The calculated results are: $V_0 = 532.69 \text{ \AA}^3$, $a = 6.50 \text{ \AA}$, $b = 10.96 \text{ \AA}$, and $c = 7.53 \text{ \AA}$, which are in good agreements with experimental results: $V_0 = 523.91 \text{ \AA}^3$, $a = 6.54 \text{ \AA}$, $b = 11.05 \text{ \AA}$, and $c = 7.37 \text{ \AA}$.²¹

C. The CS-RD procedure

The CS-RD computational protocol¹⁰ uses RD simulations at constant shear rate on uniaxial compressed HMX single crystal to determine how the physical and chemical responses depend on compression direction and slip system. CS-RD was designed as a rapid assay to distinguish shock directions likely to be sensitive from those likely to be less sensitive. Thus, we chose an initial compressive strain that induces impact stresses sufficiently large to initiate rapid shear deformation but small enough that anisotropic sensitivity can be distinguished. With these relatively large impact stresses, we can quickly evaluate the changes of stresses, temperature, and chemistry as the shock induced shear stress deforms and breaks molecules in slip planes during the constant-rate shear deformation imposed on system. Thus, the differences among various slip systems along different shock directions can be quickly distinguished based on molecular responses to shear deformation. Important differences in molecular responses are found to appear within the first few picoseconds during CS-RD simulations, making it practical to consider many slip systems

to find the ones requiring the least stress to initiate shear dynamics.

The steps of CS-RD simulation are as follows:

1. Uniaxial compression along specific shock direction. The unit cell was first uniaxially compressed by 17% along each of the three shock directions (in this paper normal to (110), (011), and (010) planes).
2. Relaxation of the compressed system. The compressed unit cells were expanded to $4 \times 2 \times 3$ supercells, which were then energy-minimized and equilibrated with fixed cell parameters using reactive dynamics for 2 ps at $T = 300$ K (denoted as NVT-RD). At the end of this relaxation, the pressures are 11.5 ± 0.5 GPa, 9.6 ± 0.4 GPa, and 9.4 ± 0.5 GPa for (110), (011), and (010) planes, respectively, which correspond to the pressure of about 10 GPa in shock experiments on HMX. The difference in initial pressures induced by same amount of compression along different shock directions is arisen from anisotropic compressibility of HMX. Although the initial pressures are slightly different for the three shock directions, it is not necessary to refine it to obtain equal stresses because it is the maximum shear stress minus the equilibrium shear stress used to evaluate relative sensitivity for different shock directions, which depends little on initial stress.
3. Prediction of resolved shear stresses (RSS). The full stress tensor induced by uniaxial compression along each shock direction was calculated from the last MD snapshot and then projected onto various slip systems, a combination of slip plane and slip direction, to obtain RSS for each slip system. The most favorable slip systems for activation will be those with larger RSS, lower critical RSS and

smaller Burgers vectors.¹⁰ RSS is the driving force for potential shear deformation through slip system, suggesting that likely slip systems should be those with larger RSS. This strategy was motivated by Plaksin²² experiments, which showed clear-cut experimental evidence that initiation of detonation occurs preferentially in directions with maximum shear stresses. We calculated RSS of several slip systems for the compressed crystals along the three shock directions and then selected six systems with larger RSS to examine further. RSS of another seven slip systems observed experimentally^{23–26} were also calculated. Table I summarizes the calculated RSS for the selected thirteen slip systems.

4. Redefinition of compressed unit cell. For each of the thirteen slip systems, the compressed unit cell is redefined and reoriented to make the new x axis along slip direction and the new x - z plane as slip plane. The unit cell parameters and number of molecules per unit cell after redefinition for each slip system are included in Table I of the supplemental materials.³⁵ The redefined systems were then relaxed with fixed cell parameters to minimize energy and equilibrated at $T = 300$ K by performing NVT-RD simulation for 2 ps. Then the equilibrated cells for the thirteen slip systems were expanded to larger supercells, which are summarized in Table I of the Supplemental Materials. Take (111) \langle 01-1 \rangle slip system along shock direction normal to (110) plane for example, $8 \times 8 \times 2$ unit cells were used in the a , b , and c directions, leading to 1536 molecules and 43 008 atoms. The dimensions of the supercell are $103.36 \text{ \AA} \times 102.12 \text{ \AA} \times 39.03 \text{ \AA}$ along the a , b , and c directions. NVT-RD simulation at $T = 300$ K was next carried out for each supercell for 1 ps.
5. Shear deformation dynamics. Finally, nonequilibrium reactive dynamics (NE-RD) was applied to simulate shear deformation for each compressed and reoriented crystal for 8 ps at a constant shear rate of 0.5/ps along x direction in x - z plane. A schematic illustration of the supercell for CS-RD simulation is shown in Fig. 1. This deformation was carried out uniformly with the supercell strained equally at each MD time step (0.1 fs). Full periodic boundary conditions were used in all simulations.

TABLE I. Thirteen potential slip systems along three shock directions normal to (110), (011), and (010) planes including resolved shear stress and shear stress barrier. The eight slip systems in bold font are preferred according to larger resolved shear stress.^a

Shock plane	Slip system	S_{xy} (GPa)	$\tau_{max} - \tau_0$ (GPa)
(110)	(100)\langle010\rangle	2.35	2.51
	(111)\langle01-1\rangle	1.62	3.24
	(011) \langle 11-1 \rangle ^{b,c}	0.99	3.93
	(101) \langle 10-1 \rangle ^{d,e}	0.86	4.20
	(001) \langle 100 \rangle ^d	0.06	5.36
(011)	(001)\langle010\rangle	2.15	2.88
	(101)\langle010\rangle	2.07	3.14
	(111)\langle1-10\rangle	1.47	2.84
	(001) \langle 100 \rangle ^d	0.94	4.26
	(101) \langle -101 \rangle ^{d,e}	0.71	4.05
(010)	(100)\langle001\rangle	3.47	3.00
	(001)\langle100\rangle^d	3.22	2.72
	(011)\langle11-1\rangle^{b,c}	2.14	2.46

^aShock plane: the normal is parallel to shock direction; S_{xy} : resolved shear stress; $\tau_{max} - \tau_0$: shear stress barrier, τ_0 is initial shear stress, τ_{max} is the maximum shear stress.

^bFrom Ref. 23.

^cFrom Ref. 24.

^dFrom Ref. 25.

^eFrom Ref. 26.

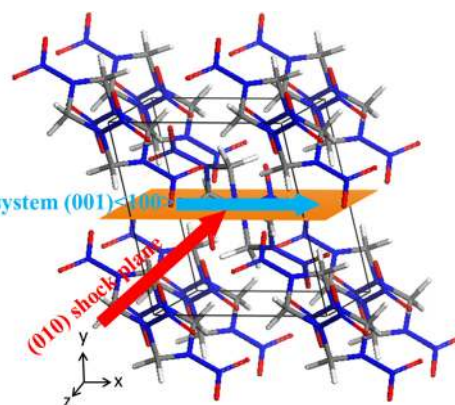


FIG. 1. The CS-RD model for HMX single crystal. Shown is the case of 17% pre-compression along shock direction normal to (010) plane with constant shear rate in \langle 100 \rangle slip direction (along x direction) on (001) slip plane (parallel to x - z plane). In this case, shock plane is perpendicular to slip plane.

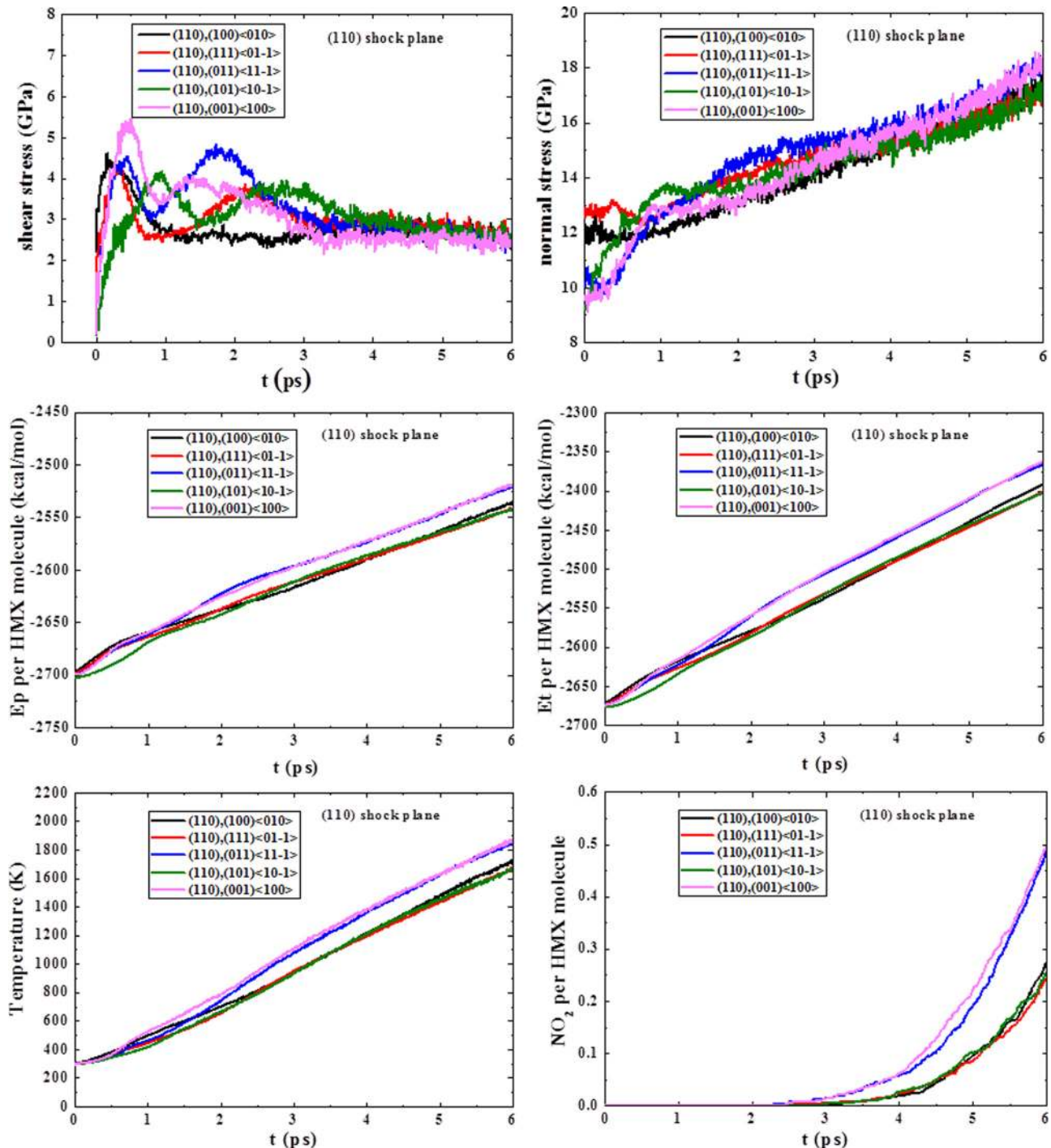


FIG. 2. Time evolutions of shear stress, normal stress, potential energy, total energy, temperature, and NO_2 formation for five slip systems along shock direction normal to (110) plane during CS-RD simulations. (100) \langle 010 \rangle and (111) \langle 01-1 \rangle slip systems lead to lower shear stress barriers making them the two preferred slip systems.

III. RESULTS AND DISCUSSION

A. Prediction of preferred slip systems

1. Shock direction normal to (110) plane

Five likely slip systems along shock direction normal to (110) plane were selected based on larger RSS and experiments^{23–26} to simulate the shear deformation. The calculated RSS included in Table I indicate that (100) \langle 010 \rangle and (111) \langle 01-1 \rangle slip systems are more likely to slip than the

other three due to larger RSS. Preferred slip system are expected to be the one with the minimum shear stress barrier, the maximum shear stress minus the initial shear stress ($\tau_{max} - \tau_0$), since it requires the least stress to overcome the barrier and initiate slip motion. The initial shear stress barriers included in Table I suggest that (100) \langle 010 \rangle and (111) \langle 01-1 \rangle slip systems are preferred slip systems due to smaller shear stress barriers compared with other three. This is consistent with the RSS prediction that the slip systems with higher RSS are more likely to slip.

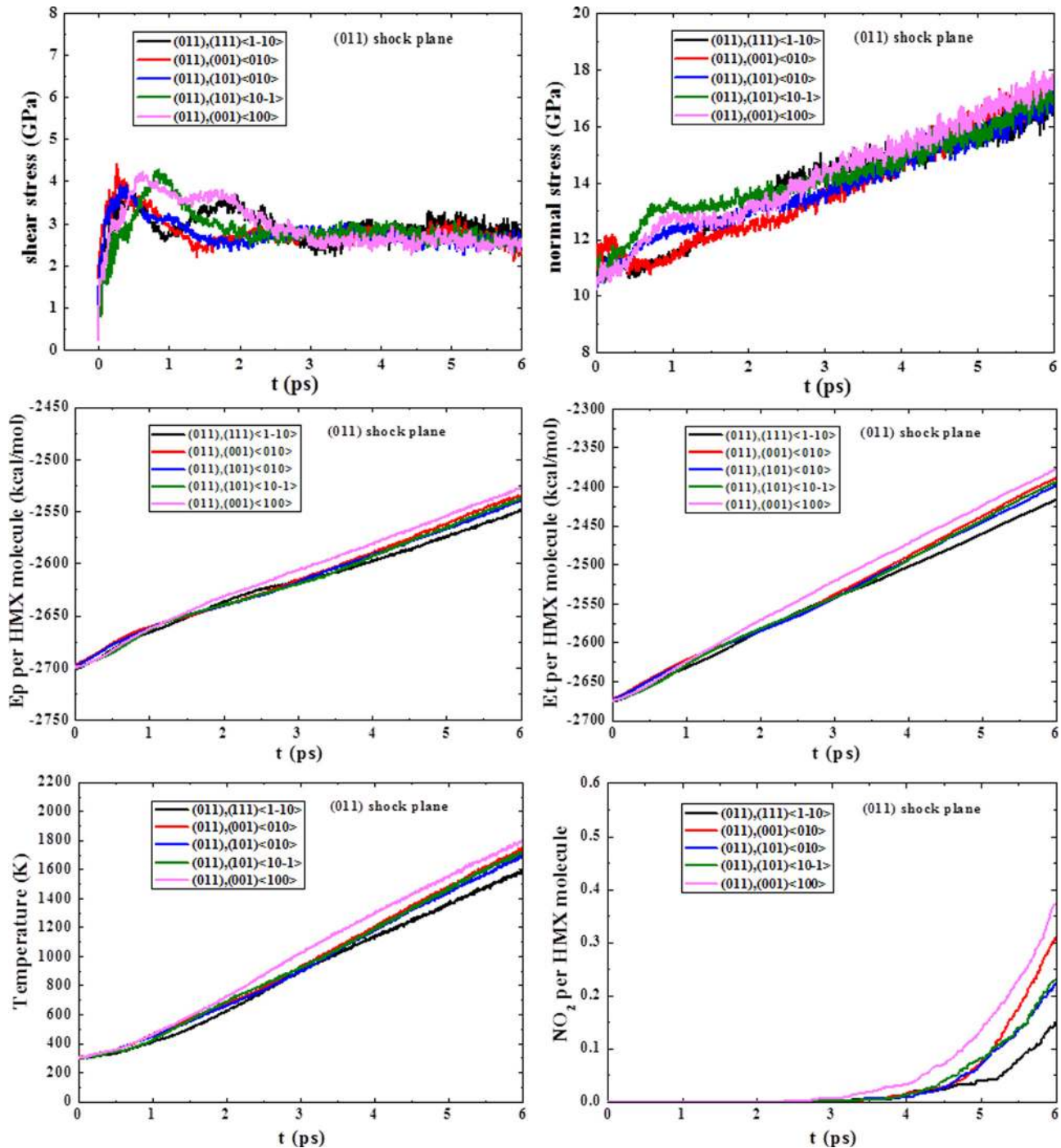


FIG. 3. Time evolutions of shear stress, normal stress, potential energy, total energy, temperature, and NO_2 formation for five slip systems along shock direction normal to (011) plane during CS-RD simulations. The small shear stress barriers for (001)010, (101)010, and (111)1-10 slip systems suggest that these three are preferred slip systems.

Time evolutions of shear stress, normal stress, energy, temperature, and main reaction product NO_2 for the five slip systems during the CS-RD simulations are shown in Fig. 2. Shear stresses reach the initial peaks earlier and then decrease more quickly for the two preferred slip systems than the other three. No or small second shear stress barriers appear for the two preferred slip systems, whereas, a large second shear stress barrier appears for each non-preferred slip system, indicating that it is hard to shear in these three slip systems as a second large shear stress barrier must be

overcome. Moreover, RSS for these three slip systems are small such that they would not provide enough driving force to overcome the big hindrance to shear. (100)010 slip system is the most preferred one due to the lowest shear stress barrier.

2. Shock direction normal to (011) plane

Five likely slip systems along shock direction normal to (011) plane were identified according to larger RSS and

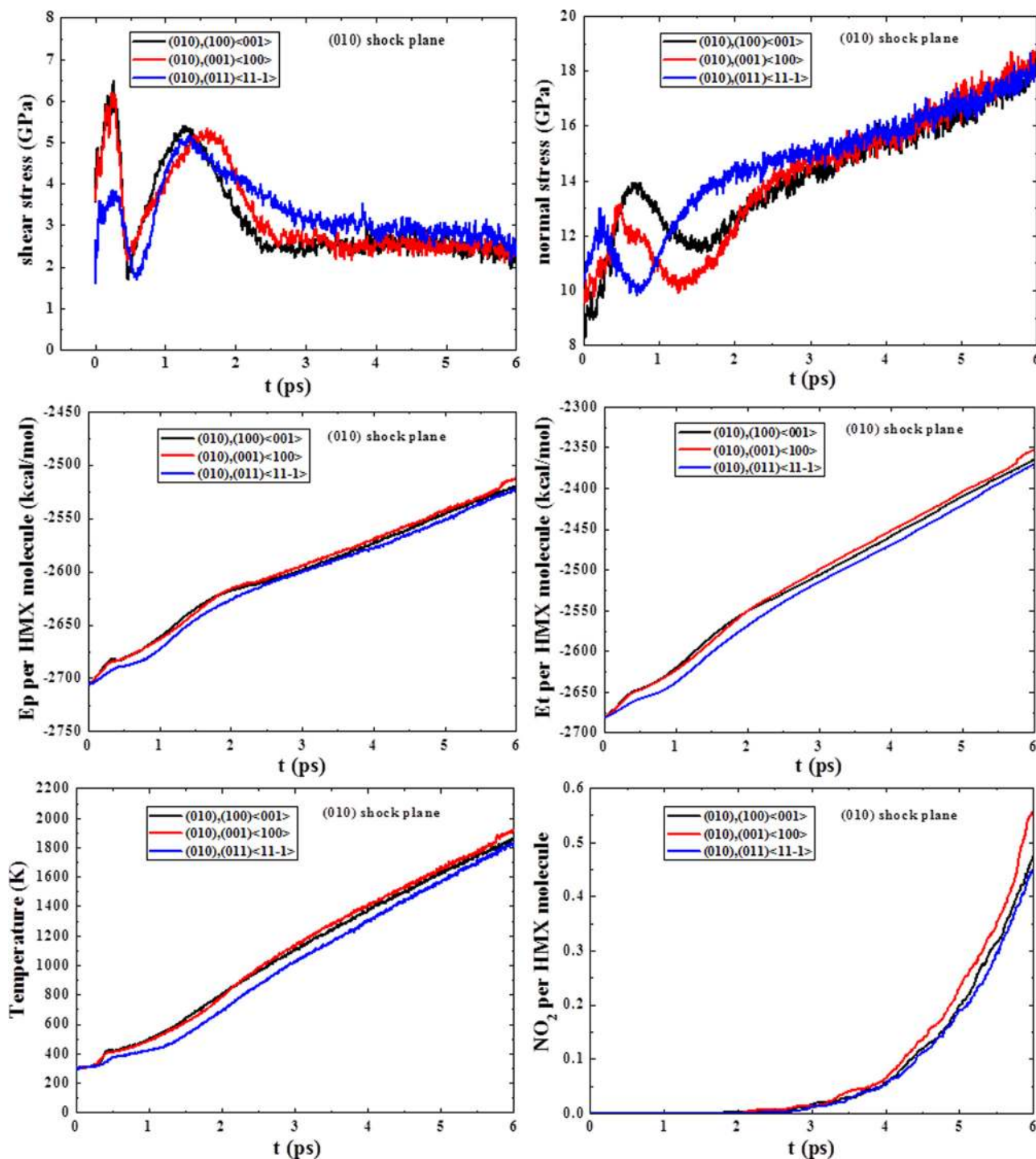


FIG. 4. Time evolutions of shear stress, normal stress, potential energy, total energy, temperature, and NO_2 formation for three slip systems along shock direction normal to (010) plane during CS-RD simulations. The low shear stress barriers for the three slip systems indicate that all of them are favorable.

experiments.^{25,26} The calculated RSS presented in Table I indicate that (001)⟨010⟩, (101)⟨010⟩, and (111)⟨1-10⟩ slip systems are more likely to slip than the other two because of higher RSS. These predictions from larger RSS are confirmed by the initial shear stress barriers included in Table I, which suggest that (001)⟨010⟩, (101)⟨010⟩, and (111)⟨1-10⟩ slip systems are preferred arising from smaller shear stress barriers. Fig. 3 shows the time evolutions of shear stress, normal stress, energy, temperature, and main reaction product NO_2 for the five slip systems during CS-RD simulations. Shear stress approaches to

the peak earlier and then decreases more quickly for each preferred slip system than the other two. (111)⟨1-10⟩ slip system is the most preferred one because of the lowest shear stress barrier.

3. Shock direction normal to (010) plane

Three possible slip systems along shock direction normal to (010) plane were chosen on the basis of larger RSS and experiments.²³⁻²⁵ The large RSS included in Table I

TABLE II. Eight preferable slip systems along three shock directions including shear stress barrier, shear stress overshoot, temperature, and NO₂ population. The three slip systems in bold font are the most preferred according to the lowest shear stress barrier to access the sensitivity of different shock directions.^a

Shock plane	Slip system	$\tau_{max}-\tau_0$ (GPa)	$\tau_{max}-\tau_c$ (GPa)	T(K)	NO ₂ per HMX (%)	Sensitivity
(110)	(100)⟨010⟩	2.51	2.15	1204	1.9	I
	(111)⟨01-1⟩	3.24	1.71	1194	2.3	
(011)	(111)⟨1-10⟩	2.84	1.21	1125	1.2	I
	(001)⟨010⟩	2.88	2.06	1202	1.5	
	(101)⟨010⟩	3.14	1.46	1190	1.0	
(010)	(011)⟨11-1⟩	2.46	2.83	1301	5.1	S
	(001)⟨100⟩	2.72	3.89	1414	6.4	
	(100)⟨001⟩	3.00	4.21	1384	5.7	

^aSensitivity: S-sensitive, I-insensitive; $\tau_{max}-\tau_c$: shear stress overshoot, τ_c is the equilibrium shear stress; Temperature and NO₂ per HMX are measured at $t = 4$ ps.

illustrate that all the three slip systems (100)⟨001⟩, (001)⟨100⟩, and (011)⟨11-1⟩ are preferred, which are validated by the low initial shear stress barriers summarized in Table I. Time evolutions of shear stress, normal stress, energy, temperature, and main reaction product NO₂ for the three slip systems during CS-RD simulations are shown in Fig. 4. The physical and chemical responses to shear deformation for (100)⟨001⟩ and (001)⟨100⟩ slip systems are almost the same: the initial sharp and large shear stress barrier followed by a second large shear stress barrier, and fast increases of temperature and energy. The initial shear stress barrier for (011)⟨11-1⟩ slip system is relatively flatter and smaller and the increases of temperature and energy are slower compared with (100)⟨001⟩ and (001)⟨100⟩ slip systems. (011)⟨11-1⟩ slip system is the most preferred one resulting from the lowest shear stress barrier.

Summarily, preferred slip systems leading to lower shear stress barriers for initiating shear deformation were determined for each shock directions. Larger shear stress barriers for unfavorable slip systems are arisen mainly from stronger steric overlap of molecules, leading to faster increases of temperature and energy, as well as more reaction products. The combination of larger RSS and lower shear stress barrier provides the criteria for identifying preferred slip systems. To demonstrate that this criteria is not dependent on applied shear rate, another two CS-RD simulations at the shear rate of 1.0/ps were performed for (111)⟨1-10⟩ and (101)⟨010⟩ slip systems along shock direction normal to (011) plane. The results shown in Fig. 1 of the Supplementary Materials are similar to those at the shear rate of 0.5/ps, both of which illustrate that (111)⟨1-10⟩ slip system is more preferred than (101)⟨010⟩ slip system. These confirm that the combination of larger RSS and lower shear stress barrier is useful in predicting preferable slip systems, which is not influenced by applied shear rate.

B. Anisotropic sensitivity for various shock directions

Eight preferred slip systems along three shock directions were predicted under compression-shear loading as summarized in Table II. For clarity, only the most preferred slip system exhibiting the lowest shear stress barrier along each shock direction was used to compare sensitivity of different

shock directions. The physical and chemical responses of the three most likely slip systems to shear deformation are shown in Figs. 5(a)–5(f). The time evolutions of stress, energy, temperature, and population of NO₂ fragment are similar for the two slip systems along shock directions normal to (110) and (011) planes, which are quite different from those for (010) plane.

Figs. 5(a) and 5(b) show that the shear stress barriers for (110) and (011) planes are flat and small, resulting in gradually increases of energy and temperature. The initial shear stress barrier for (010) plane is followed by a second large shear stress barrier lasting from 0.8 ps to 4.0 ps, indicating stronger steric hindrance to slip and increased molecular deformation in this orientation. This leads to faster increases of energy and temperature as well as earlier initiation of chemical reactions for (010) plane than those for (110) and (011) planes. These results can be compared to that from plate impact experiments,¹¹ where the shock decay of the elastic shock precursors is identical for (110) and (011) orientations, whereas, (010) orientation leads to much higher elastic precursor at large propagation distance with a much lower rate of decay than others.

Comparisons of potential energy and total energy for the three shock planes presented in Figs. 5(c) and 5(d) show that energy increases much faster for (010) plane than that for (110) and (011) planes. Two fast increasing stages of energy before 2 ps appear for (010) plane to overcome the two large shear stress barriers, whereas, only one fast increasing stage before 0.5 ps appears for (110) and (011) planes to surmount flat shear stress barriers.

Two fast increasing stages of temperature for (010) plane appear after passing through the two large shear stress barriers as shown in Fig. 5(e). The temperature reaches ~ 400 K at 0.5 ps after overcoming the initial shear stress barrier and goes up to ~ 1300 K at $t = 4$ ps after completely surmounting the second large shear stress barrier. The temperatures for (110) and (011) planes increase gradually to ~ 1200 K and ~ 1100 K at $t = 4$ ps, which is 100 K and 200 K lower than that for (010) plane, respectively. This is mainly ascribed to larger second shear stress barrier for (010) plane than that for (110) and (011) planes.

Temperature is found to be an important variable controlling the chemical changes in the shock-compressed high explosives. It is the most sensitive probe for energy balance

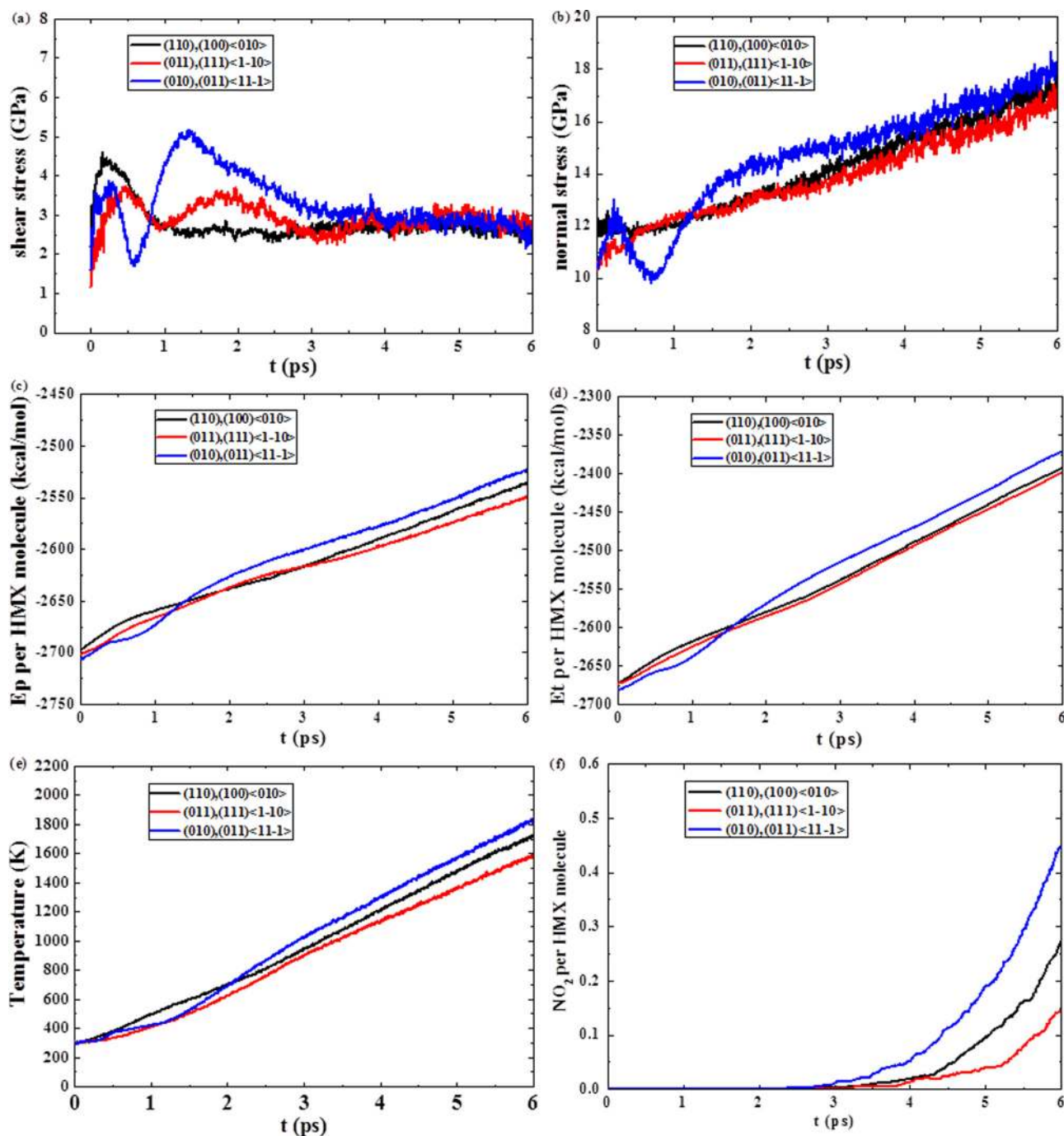


FIG. 5. Comparisons of time evolutions of shear stress, normal stress, potential energy, total energy, temperature, and NO₂ formation for the three most preferable slip systems along three shock directions during CS-RD simulations. Higher stress barriers, faster energy and temperature increases, and larger NO₂ population indicate that (010) shock plane is more sensitive than (110) and (011) shock planes.

of chemical reactions since chemical reactions rates increase quickly with temperature. The main reaction product NO₂ presented in Fig. 5(f) appears initially at $t = 2.4$ ps for (010) planes, which is about 1 ps earlier than that for (110) and (011) planes. This is explained by faster temperature increase arising from stronger intermolecular entanglement and friction during slip for (010) plane than that for (110) and (011) planes. At $t = 4$ ps, the population of NO₂ per HMX molecule reaches 0.051, 0.019, and 0.012 for (010), (110), and (011) planes, respectively, indicating that the chemical reaction rate of N-NO₂ bond breaking is faster for (010) plane than that for (110) and (011) planes.

The rates of energy and temperature increases and chemical reaction initiation within the first 2–4 ps of overcoming the shear stress barriers are most critical for differentiating sensitivity of different shock directions. Based on the time evolutions of stress, energy, temperature, and reaction product during this period, we conclude that (010) plane is more sensitive than (110) and (011) planes, which is consistent with the weak shock experimental result on HMX.¹¹ CS-RD simulations for (011) and (010) planes at the shear rate of 1.0/ps and 0.25/ps were carried out to confirm that this conclusion is not related to how large the shear rate is. The results at the shear rate of 1.0/ps shown in

Fig. 2 and 0.25/ps in Fig. 3 in the Supplemental Materials are similar to those at the shear rate of 0.5/ps, all of which show that (010) plane is more sensitive than (011) plane. Thus, the sensitivity of different shock planes is not affected by applied shear rate.

For PETN a direct relationship between shear stress overshoot, the maximum shear stress minus the equilibrium shear stress ($\tau_{max}-\tau_c$), and sensitivity was found: larger shear stress overshoot corresponds to more sensitive shock direction.¹⁰ Similar correlation exists for HMX. The calculated shear stress overshoots for the three shock directions included in Table II demonstrate that the order of sensitivity for the three shock planes is (010) > (110) > (011). Sensitive (010) plane reveals larger stress overshoot and faster temperature and energy increases, leading to earlier bond-breaking and faster N-NO₂ dissociation, whereas, less sensitive (110) and (011) planes exhibit smaller stress overshoots, lower temperature and energy increases, as well as delayed bond dissociation.

Note that continuing the constant-rate shear simulation at the same high rate for long time eventually heats all systems up to sufficiently high temperatures that reactions are initiated. Under such conditions, shocks along all three directions would likely lead to detonations eventually, however, our goal here is to quickly learn about the relative sensitivity along different directions. Thus for a rapid assay of sensitivity, we choose conditions under which just a few picoseconds can distinguish directions likely to be sensitive from those that are not likely. Here, just 4 ps of simulations show important differences between sensitive and less sensitive directions. These results on HMX and the earlier ones on PETN, the two systems with the least ambiguous experimental data on sensitivity for different shock directions, validate this CS-RD protocol.

C. Two stages of the compressive-shear process

Two stages were observed during the constant-rate shear deformation. The first stage ($t < 2$ ps) leads only to physical interactions between molecules, with no chemical reactions were observed. Intermolecular contact between slipping planes causes fast increases of shear and normal stresses, leading to a large amount of work being done on system with concomitant rises of temperature and energy. During this time, molecules get most jammed together until the maximum shear stress is reached, at which point they relax back as the planes slide further, leading to a jump in temperature and an additional increase in normal stress. The time evolution of microstructure before 2 ps for (011)(11-1) slip system along shock direction normal to (010) plane can be accessed in the Supplemental Materials named 2ps.xyz, which shows molecular deformation prior to bond-breaking and decomposition.

Physical differences between sensitive (010) plane and less sensitive (110) and (011) planes are obvious during the first stage of shear deformation. (010) plane exhibits two fast increasing stages of energy and temperature resulting from sharp and large shear stress barriers, whereas, (110) and (011) planes reveal gradually increases of temperature and energy due to flat and small shear stress barriers (see Fig. 5). These demonstrate that close intermolecular contact between

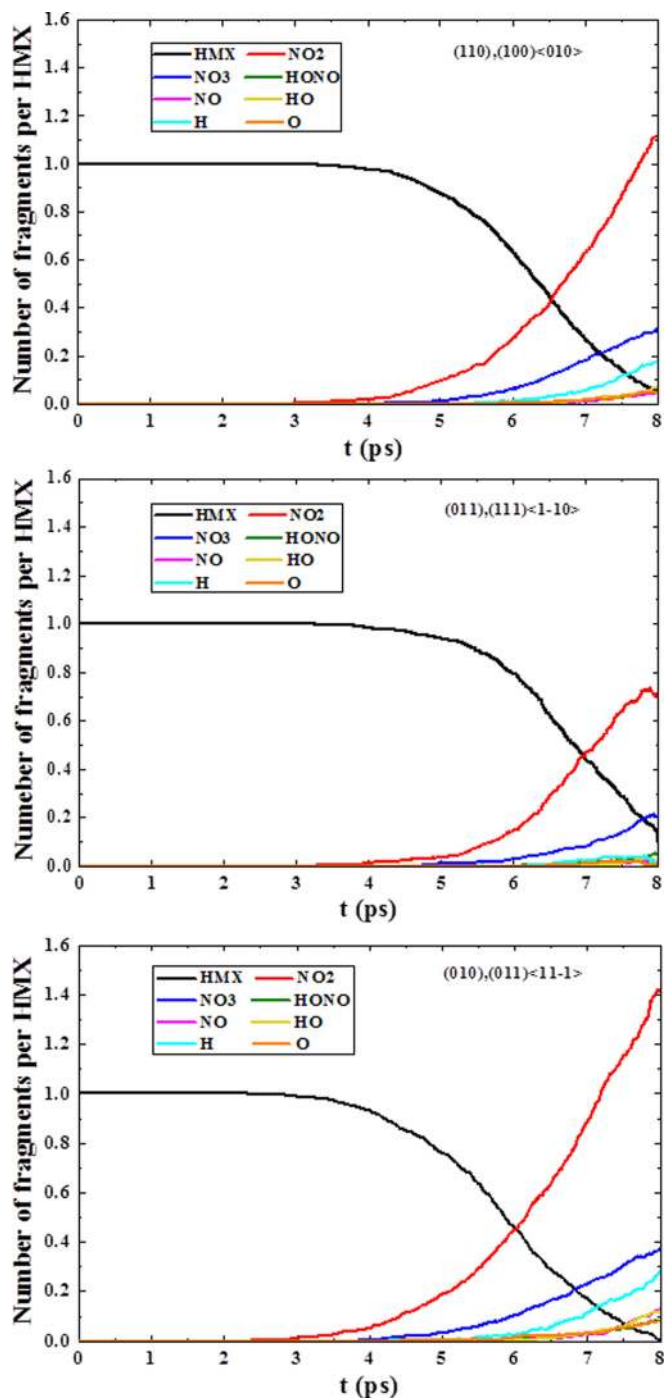


FIG. 6. Time evolutions of main products during CS-RD simulations for the three most preferable slip systems along three shock directions. Chemical reactions proceed more quickly for sensitive (010) shock plane with more products formed in shorter time compared with less sensitive (110) and (011) shock planes.

slip planes for sensitive direction results in considerably larger jumps in stresses, energy, and temperature.

It is interesting to note that the increase of potential energy appears earlier and goes faster than that of kinetic energy as well as temperature. Potential energy increases as the system moves up the shear stress barrier due to physical deformations of molecules, leading to internal energy changes of intramolecular interactions (like bond, angle, and dihedral) along with intermolecular interactions (like van der

Waals). Friction and extrusion between adjacent molecules during slip lead to the increases of temperature and kinetic energy, which approach to local maximums as the system has surmounted shear stress barriers.

In the second stage ($t > 2$ ps), chemical reactions initiations occur, leading to the formations of various products as shown in Fig. 6. Previous experiments using thermogravimetric modulated beam mass spectrometry and isotope scrambling identified gaseous pyrolysis products of condensed HMX decomposition such as HCN, CO, CH₂O, NO, N₂O, and H₂O at low temperature (< 1000 K).^{27–29} Previous theoretical studies of various decomposition channels of the gas-phase HMX molecule include N-NO₂ bond dissociation, HONO elimination, and the concerted ring fission.^{30–32} Manaa *et al.*³³ investigated the chemistry of HMX at temperature of 3500 K using a quantum molecular dynamics simulation and suggested that the first chemical event is the breaking of the N-NO₂ bond followed by the C-N bond breaking. Recently, Zhu *et al.*³⁴ performed *ab initio* molecular dynamics simulations in conjunction with multiscale shock technique to study the initial chemical processes of HMX under shock wave loading, showing that the initial decomposition of shocked HMX is triggered by N-O bond breaking and ring opening. During the CS-RD simulations, the initial chemical reaction is found to be N-NO₂ bond dissociation, which is consistent with the results from Refs. 30–33. Other species (such as NO₃, HONO, NO, HO, H, O, etc.) appear subsequently as the chemical reactions proceed, but the quantities are much smaller than that for NO₂. Final products, like H₂O and N₂, appear but with small amounts due to short simulation time.

Chemical reactions proceed more quickly for sensitive (010) plane with more products formed in shorter time compared with less sensitive (110) and (011) planes. The N-NO₂ bond breaking observed at $t = 2.4$ ps for (010) plane is delayed about one picosecond for (110) and (011) planes due to slower temperature increase. The populations of small fragments, such as HO, NO, H, and O, are larger for sensitive (010) plane than that for less sensitive (110) and (011) planes, indicating that stronger intermolecular contact and/or friction for (010) plane accelerate the dissociations of small fragments, particularly, the atoms in contact with molecules in adjacent slip planes. By the end of the simulations, 8 ps, no HMX molecule survives for (010) plane, whereas, about more than 10% HMX molecules still present for (110) and (011) planes.

Shear viscosity was calculated from converged shear stress at $t = 6$ ps of the amorphous system using $\tau_{xy} = \eta \dot{\gamma}_{xy}$, where τ_{xy} is the equilibrium shear stress (GPa), $\dot{\gamma}_{xy}$ is the shear rate 0.5 ps^{-1} , and η is viscosity in unit of Pa·S. The predicted viscosity is about 0.005 Pa·S for all three shock directions.

IV. CONCLUSIONS

The physical and chemical responses of single crystal HMX to combined compression and shear loading were studied using CS-RD computational protocol with ReaxFF-*lg* reactive force field. The CS-RD model predicts distinct differences in physical and chemical responses along different

compression directions, demonstrating that shock direction normal to (010) plane is more sensitive than shock directions normal to (110) and (011) planes. This is consistent with shock experiments providing additional validation of the CS-RD model. The origin of this difference in sensitivity is the large shear stress barriers arising from steric overlap of molecules in adjacent slip planes during shear motion induced by shock direction normal to (010) plane. This leads to great deformation of molecules and higher energy concentration in the shear localized region, resulting in large temperature rise. Temperature rising and severe molecular deformation accelerate initial chemical bond breaking that induces further decomposition, eventually leading to detonation.

The larger RSS criterion provides a way to identify probable slip systems. Slip systems exhibit larger RSS show lower shear stress barriers during shear deformation, making them easier to slip. A direct relationship between sensitivity of different shock directions and shear stress overshoot is found, namely, larger shear stress overshoot corresponds to more sensitive shock direction.

Now that the CS-RD model has been validated to interpret sensitivity for both HMX and PETN, we suggest that this approach should be valuable for studying sensitivity of more complex systems containing grain boundaries, polymers, voids, and inclusions to assess the impact of these defects for detonation.

Stress that the CS-RD method is designed for rapidly distinguishing sensitive direction from those that are likely to be less sensitive. Thus, the relatively large initial shock compression and shear rate were chosen such that allowing shear deformation to propagate for just few picoseconds already distinguishes between sensitive and less sensitive. Such huge energy inputs would soon lead to decomposition for all shock directions under continuing shear deformation. However, in the first 2 ps, we see clearly that sensitive direction requires larger shear stress to slip planes (due to bad steric contacts) followed by faster increases of temperature and energy, which leads to earlier molecular decomposition over the next 2 to 4 ps. For more realistic shock simulations of the initiation of detonation and sensitivity, we might have to consider simulation times 100 or 1000 times longer for the system sizes that are 100 or 1000 times larger. Such simulations are becoming possible on the supercomputers and will likely be done over the next few years. But in the meantime we need to identify issues that may play important roles in controlling sensitivity.

ACKNOWLEDGMENTS

This work was supported by the U.S. Army Research Office (W911NF-05-1-0345 and W911NF-08-1-0124; Ralph Anthenien program manager) and by Office of Naval Research (N00014-09-1-0634; Cliff Bedford program manager). It was also supported by the National Natural Science Foundation of China (Grant No. 10832003) and by the Open Grant of State Key Laboratory of Explosion Science and Technology, Beijing Institute of Technology, P. R. China (Grant No. KFJJ12-6M). Some computations in this work were carried out on the Army HPC system (the Arctic

Region Supercomputer Center) (we thank Dr. Betsy Rice and Larry Davis for assistance).

- ¹Y. M. Gupta, *J. Phys.* IV **C4**, 345 (1995).
- ²R. Cheret, *Detonation of Condensed Explosives* (Springer, New York, 1993).
- ³C. S. Yoo, N. C. Holmes, P. C. Souers, C. J. Wu, F. H. Ree, and J. J. Dick, *J. Appl. Phys.* **88**, 70 (2000).
- ⁴D. D. Dlott and M. D. Fayer, *J. Phys. Chem.* **92**, 3798 (1990).
- ⁵C. S. Yoo, Y. M. Gupta, and P. D. Horn, *Chin. Phys. Lasers* **159**, 178 (1989).
- ⁶S. A. Sheffield, R. Engelke, and R. R. Alcon, in *Proceedings of the Ninth International Symposium on Detonation, Portland, Oregon* (Office of Naval Research, Arlington, VA, 1989), p. 39.
- ⁷J. J. Dick, *Appl. Phys. Lett.* **44**, 859 (1984).
- ⁸J. J. Dick, R. N. Mulford, W. J. Spencer, D. R. Pettit, E. Garcia, and D. C. Shaw, *J. Appl. Phys.* **70**, 3572 (1991).
- ⁹J. J. Dick and J. P. Ritchie, *J. Appl. Phys.* **76**, 2726 (1994).
- ¹⁰S. V. Zybin, W. A. Goddard III, P. Xu, A. C. T. van Duin, and A. P. Thompson, *Appl. Phys. Lett.* **96**, 081918 (2010).
- ¹¹J. J. Dick, D. E. Hooks, R. Menikoff, and A. R. Martinez, *J. Appl. Phys.* **96**, 374 (2004).
- ¹²R. Menikoff, J. J. Dick, and D. E. Hooks, *J. Appl. Phys.* **97**, 023529 (2005).
- ¹³L. C. Liu; Y. Liu; S. V. Zybin, and W. A. Goddard III, *J. Phys. Chem. A* **115**(40), 11016 (2011).
- ¹⁴A. Strachan, A. C. T. van Duin, D. Chakraborty, S. Dasgupta, and W. A. Goddard III, *Phys. Rev. Lett.* **91**, 098301 (2003).
- ¹⁵A. Strachan, E. Kober, A. C. T. van Duin, J. Oxgaard, and W. A. Goddard III, *J. Chem. Phys.* **122**, 054502 (2005).
- ¹⁶A. Nakano, R. K. Kalia, K. Nomura, A. Sharma, P. Vashishta, F. Shimojo, A. C. T. van Duin, W. A. Goddard III, R. Biswas, and D. Srivastava, *Comput. Mater. Sci.* **38**, 642 (2007).
- ¹⁷K. Nomura, R. K. Kalia, A. Nakano, and P. Vashishta, *Appl. Phys. Lett.* **91**, 183109 (2007).
- ¹⁸A. C. T. van Duin, Y. Zeiri, Y. F. Dubnikova, R. Kosloff, and W. A. Goddard III, *J. Am. Chem. Soc.* **127**, 11053 (2005).
- ¹⁹L. Zhang, S. V. Zybin, A. C. T. Van Duin, S. Dasgupta, W. A. Goddard III, and E. M. Kober, *J. Phys. Chem. A* **113**, 10619 (2009).
- ²⁰T. T. Zhou, Y. Liu, S. V. Zybin, F. L. Huang, and W. A. Goddard III, "Equations of state of HMX polymorphs and molecular conformation transformations from ReaxFF-*lg* molecular dynamics" (to be published).
- ²¹Y. Kohno, K. Maekawa, N. Azuma, T. Tsuchioka, T. Hashizume, and A. Imamura, *Kogyo Kayaku* **53**, 227 (1992).
- ²²I. Plaksin, J. Campos, R. Mendes, J. Ribeiro, J. Direito, D. Braga, and C. S. Coffey, in *Shock Compression of Condensed Matter-2003: Proceedings of the Conference of the American Physical Society Topical Group on Shock Compression of Condensed Matter*, 20 July (American Institute of Physics, 2004), Vol. 706, pp. 1013–1016.
- ²³S. J. P. Palmer and J. E. Field, *Proc. R. Soc. London, Ser. A* **383**, 399 (1982).
- ²⁴H. H. Cady, in *Structure and Properties of Energetic Materials*, edited by D. H. Liebenberg, R. W. Armstrong, and J. J. Gilman (Materials Research Society, Pittsburgh, 1982), p. 243.
- ²⁵D. B. Sheen, J. N. Sherwood, H. G. Gallagher, A. H. Littlejohn, and A. Pearson, "Final Report to the U. S. Office of Naval Research, An Investigation of Mechanically Induced Lattice defects in Energetic Materials (University of Strathclyde, Glasgow, 1993), pp. 53 ff.
- ²⁶R. W. Armstrong, H. L. Ammon, Z. Y. Du, W. L. Elban, and X. J. Zhang, in *Structure and Properties of Energetic Materials*, edited by D. H. Liebenberg, R. W. Armstrong, and J. J. Gilman (Materials Research Society, Pittsburgh, 1982), p. 227.
- ²⁷R. Behrens, *J. Phys. Chem.* **94**, 6706 (1990).
- ²⁸R. Behrens, *Int. J. Chem. Kinet.* **22**, 135 (1990).
- ²⁹R. Behrens and S. Bulusu, *J. Phys. Chem.* **95**, 5838 (1991).
- ³⁰C. F. Melius, *Chemistry and Physics of Energetic Materials*, edited by D. N. Bulusu (Kluwer, Dordrecht, The Netherlands, 1990).
- ³¹J. P. Lewis, K. R. Glaesemann, K. VanOpdorp, and G. A. Voth, *J. Phys. Chem. A* **104**, 11384 (2000).
- ³²D. Chakraborty, R. P. Muller, S. Dasgupta, and William A. Goddard III, *J. Phys. Chem. A* **105**, 1302 (2001).
- ³³M. R. Manaa, L. E. Fried, C. F. Melius, M. Elstner, and Th. Frauenheim, *J. Phys. Chem. A* **106**, 9024 (2002).
- ³⁴W. H. Zhu, H. Huang, H. J. Huang, and H. M. Xiao, *J. Chem. Phys.* **136**, 044516 (2012).
- ³⁵See supplementary material at <http://dx.doi.org/10.1063/1.4729114> for unit cell parameters, number of molecules per unit cell after redefinition and the size of supercell for each of the thirteen slip systems during CS-RD simulations in Table I; microstructure evolution before 2 ps during CS-RD simulation for (011)(11-1) slip system along the shock direction normal to (010) plane named 2ps.xyz; time evolutions of shear stress, normal stress, potential energy, total energy, temperature, and NO₂ formation of (111)(1-10) and (101)(010) slip systems for (011) shock plane during CS-RD simulations at the shear rate of 1.0/ps in Fig. 1; comparisons of time evolutions of shear stress, normal stress, potential energy, total energy, temperature, and NO₂ formation of the two most preferable slip systems for (011) and (010) shock planes during CS-RD simulations at the shear rate of 1.0/ps in Fig. 2 and 0.25/ps in Fig. 3.